Impact of CHAMP Radio Occultation Observations on Global Analysis and Forecasts in the Absence of AMSU Radiance Data

X. ZOU, H. LIU

Florida State University, Tallahassee, Florida, USA

R.A. ANTHES

University Corporation for Atmospheric Research, Boulder, Colorado, USA

H. SHAO

Florida State University, Tallahassee, Florida, USA

J.C. CHANG

Chinese Culture University, Taipei, Taiwan

and

Y.-J. ZHU

National Centers for Environmental Prediction, Camp Springs, Maryland, USA

(Manuscript received 13 June 2003, in revised form 11 November 2003)

Abstract

Challenging Minisatellite Payload (CHAMP) radio occultation (RO) observations during a two-week period are assimilated into global analyses using the National Center for Environmental Prediction (NCEP) three-dimensional variational (3D-Var) system with a recently improved observation operator for assimilating GPS bending angle data. The NCEP 3D-Var system used in this research is suboptimal since Advanced Microwave Unit (AMSU) radiances are not included in our experiments. Analyses with and without CHAMP observations are compared with each other and with collocated conventional radiosonde and dropsonde data, which are excluded from both experiments. Zonal mean temperature, humidity and surface pressure differences between the GPS analyses and NO-GPS analyses are examined. The GPS analyses in the Southern Hemisphere show higher temperatures than the NO-GPS analyses, particularly in the mid- and high latitudes. The GPS analyses show drier air in the lower troposphere and more moist air in the middle troposphere compared to the NO-GPS analyses. The surface pressure is slightly increased (maximum 0.8 hPa) in the Southern Hemisphere and decreased (maximum 0.25 hPa)

Corresponding author: Xiaolei Zou, Department of Meteorology, Florida State University, 404, Love Bldg, Tallahassee, Florida, 32306-4520, USA.
E-mail: zou@met.fsu.edu

in the Northern Hemisphere due to the inclusion of GPS observations. Compared with the collocated independent soundings, the large cold bias (as large as 2.5 K) in the NCEP Southern Hemisphere analyses produced without CHAMP observations is significantly reduced. On average, a 20% mean error reduction in the temperature analysis is obtained in the Southern Hemisphere when CHAMP data are included. Degradations in the surface pressure analysis found from previous the GPS/Meteorology data assimilation studies are greatly reduced. The differences between the surface pressure analysis errors with and without CHAMP data are less than 0.8 ± 1.5 hPa. Comparisons of numerical forecasts initialized with analyses produced with and without CHAMP occultations display a small improvement in the forecasts in the tropics and the Southern Hemisphere associated with the use of the CHAMP observations.

1. Introduction

Following the pioneering satellite mission that demonstrated the Global Positioning System (GPS) radio occultation (RO) technique to produce global soundings of the Earth's atmosphere—the GPS/Meteorology (GPS/MET) experiment (Ware et al. 1997), the German/US CHAMP (Challenging Minisatellite Payload) mission was launched on July 15, 2000, and RO measurements from CHAMP began on February 11, 2001 (Wickert et al. 2001). CHAMP carries the latest generation JPL (Jet Propulsion Laboratory) GPS receiver, BlackJack, which provides improved signal quality and allows for application of advanced signal tracking techniques (Yunck et al. 2000). The penetration of occultations into the lowest 1/2 km of the atmosphere over the entire globe has increased from about 30% for the GPS/MET experiment to almost 50% for CHAMP (Hajj et al. 2003). Having high vertical resolution (0.1–1 km) and high accuracy (< 1 K for temperature, 0.5 g kg^{-1} for specific humidity) under virtually all weather conditions (Hajj et al. 2003), GPS occultations are unique and complement other satellite observations, which often have high horizontal resolution, but lower vertical resolution. Assimilation of GPS RO measurements in global analyses has great potential to contribute to climate monitoring, weather forecasting and atmospheric research.

Considerable effort has been made to develop techniques for assimilating RO data into numerical weather prediction (NWP) models. Various strategies for assimilating data were discussed by Eyre (1994) and Kuo et al. (2000). Kursinski et al. (2000) combined occultation refractivity profiles from GPS/MET data with ECMWF (European Centre for Medium-Range Weather Forecasts) global analyses in a 1D-Var framework. Healy and Eyre (2000) tested the same strategy in a simulated approach. And more recently, Poli et al. (2002) explored this option with the finite volume DAO's DAS background. Palmer et al. (2000, 2001) proposed to assimilate GPS bending angle data using a forward Abel transform. Von Engeln et al. (2003) basically took the same route to probe the retrieval sensitivity with a 1D-Var tool. Zou et al. (1999, 2000), Liu et al. (2001), and Shao and Zou (2003) used a ray-tracing procedure for the assimilation of GPS/MET bending angles. It has been found that the moisture analysis, after the assimilation of GPS/MET refractivity profiles, is in general drier than the original analysis (Kursinski et al. 2000; Palmer et al. 2001). Interestingly, the comparisons with radiosondes can either be wetter (Palmer et al. 2001) or drier (Poli et al. 2002), with different backgrounds and/or approaches. Large profile-to-profile temperature discrepancies were also found in the tropical lower stratosphere due to real waves (probably gravity waves, e.g., Tsuda et al. 2000) that were not represented in the ECMWF analysis (Kursinski et al. 2000). Results from assimilating GPS/MET bending angles using a ray-tracing procedure by Zou et al. (2000), Liu et al. (2001), and Shao and Zou (2003) are summarized in Section 3.1.

Following the successful demonstration of the assimilation of GPS/MET data, several challenges remain: (i) obtaining a statistical evaluation on the impact of RO measurements to global analyses and forecasts, (ii) assessing the added value of RO observations to global analyses and forecasts in the presence of other observations, (iii) improving the moisture analysis in the lower troposphere with RO observations, (iv) eliminating the degradation in the surface pressure analysis from RO assimilation, and (v) developing a fast and

operationally-feasible method for the assimilation of RO occultations.

This research extends previous RO data assimilation studies to the assimilation of CHAMP data and addresses issues (i)–(iv) above. Work on the fifth challenge will be presented in a separate paper. Major differences between this study and our previous GPS data assimilation studies include the use of a higher resolution model (T170L42 instead of T62L28), CHAMP observations, other observations (excluding AMSU data), and a more accurate ray-tracing operator. The purpose of this effort is to assess the added value of RO observations to global analyses and one- to five-day forecasts.

In Section 2 we provide a brief description of CHAMP occultations. Section 3 provides an overview of the three-dimensional variational (3D-Var) data assimilation algorithm and the experimental design. In Section 4 the zonal and meridional distributions of GPS-derived temperature and moisture increments are presented, and analyses produced with and without CHAMP occultations are compared with collocated conventional observations, which are excluded from both data assimilation experiments. Forecasts from analyses produced with and without CHAMP occultations are evaluated in Section 4, and the summary and conclusions are given in Section 5.

2. CHAMP GPS radio occultation measurements

GPS RO measurements are based on the time delay of the transmitted GPS radio waves from a GPS satellite occulted behind the Earth as viewed from a low-Earth-orbiting satellite (Fjeldbo et al. 1971). The magnitude of the delay depends on the density of the Earth's atmosphere. Precise time delay measurements are converted first into an atmospheric Doppler shift measurement and then to a bending angle measurement based on satellite geometry (Melbourne et al. 1992). The bending angles can be used in a data assimilation system to improve global analyses and forecasts (Zou et al. 1999).

Improvement to global analyses and forecasts is determined by not only how RO observations are assimilated, but also by RO data availability and quality. Using a new generation of "semi-codeless" GPS receivers, accurate tracking of the GPS signals can be made by the CHAMP receiver while Anti-Spoofing (AS) is turned on, i.e., when the GPS signal is encrypted by the Department of Defense. Errors in individual temperature profiles are found to be less than 0.5 K in dry regions where $T <$ 250 K (Hajj et al. 2003). The new CHAMP receiver substantially increases the fraction of GPS occultations that reach the lower troposphere. The CHAMP mission also provides more daily occultations than the GPS/MET experiment and hence greater spatial coverage.

We use CHAMP observations from July 16th to July 31st, 2002 in this study. Details about the CHAMP data and their processing can be found from the UCAR (University Corporation for Atmospheric Research) COSMIC (Constellation Observing System for Meteorology, Ionosphere and Climate) Data Analysis and Archival Center (CDAAC) website (http://www.cosmic.ucar.edu:8080/cdaac/index.html). A total of 3030 occultations were processed and made available during this two-week period. The distribution of the processed data over this period is shown in Fig. 1. On average, about 200 occultations per day pass the internal quality control (QC) imposed by the UCAR CDAAC RO retrieval procedure. This QC procedure includes the truncation of the L1 signal, the truncation of the L2 signal while keeping the L1, and the noise reduction of bending angles at high altitudes (primarily above 30 km) using the CIRA+Q climatological data (Kirchengast et al. 1999). A more detailed description about the internal QC can be found in Kuo et al. (2003). Of those 3030 CHAMP soundings, 1427 CHAMP soundings (47% of the total) penetrated to a level below 850 hPa. No further QC has been done for the acquired bending angle profiles in our subsequent data assimilation experiments.

Information provided by CDAAC CHAMP level-2 data that are used for bending angle assimilation is listed in Table 1. The main difference between CHAMP level-2 data and GPS/MET level-2 data is that the normal direction of the occultation plane, directly provided in the GPS/MET level-2 data set, is not provided in the CHAMP level-2 data set. Instead, the azimuth angle (denoted by the parameter "az" in Table 1) is provided. However, the ray-tracing observation operator for direct assimilation of bending angle data requires the normal direc-

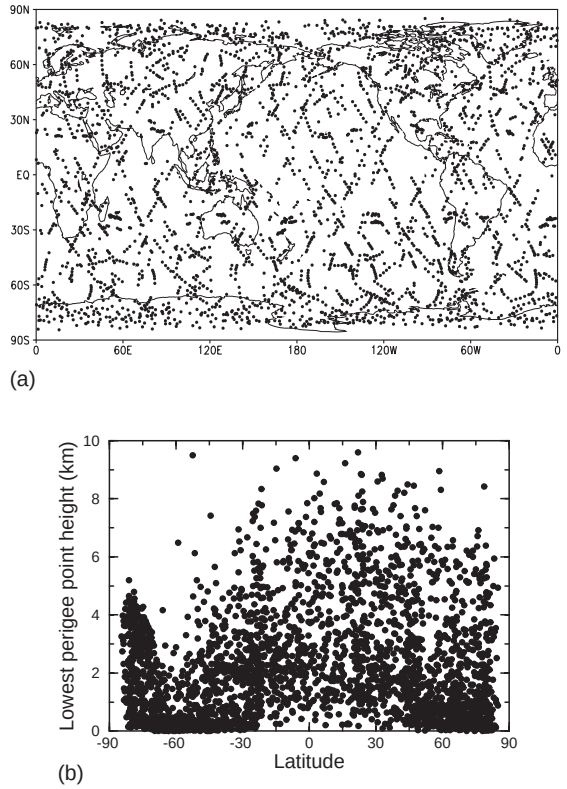

Fig. 1. (a) The locations of the 3030 CHAMP occultation profiles from July 16th to July 31st, 2002. (b) The lowest altitudes of the occultation profiles.

tion of the ray at the perigee point, which is used to derive the tangent direction for the ray integration (see Section 2 in Zou et al. 1999). Calculation of the normal direction, $\mathbf{u}_{occ}^{n}$, based on CHAMP level-2 data, is therefore required. Details of this derivation are presented in Appendix A.

3. Assimilation of GPS bending angles and experimental design

3.1 A brief review of GPS RO assimilation

The authors' efforts for assimilating GPS RO data started in 1993, before the GPS/MET launch, which occurred on April 3, 1995 (Ware et al. 1996). Zou et al. (1995) and Kuo et al. (1997) conducted two sets of observing system simulation experiments to assess the potential impact of GPS refractivity data on temperature and moisture field analysis and short-range numerical weather prediction at meso- and synoptic scales, respectively. They found beneficial impacts from assimilating refractivities for the prediction of the blizzard event of March 8, 1992 and an extratropical cyclone known as the ERICA (Experiment on Rapidly Intensifying Cyclones over the Atlantic) IOP (Intensive Observing Period) 4 storm which took place over the Northwestern Atlantic Ocean on January 4–5, 1989. Zou et al. (1999) began the development of a ray-tracing method for incorporating GPS bending angle measurements directly into a numerical weather analysis system in order to handle the complicated nonlinear dependence of the RO observations on the atmospheric refractivity along the ray path. By directly assimilating either bending angles or refractivities, the ambiguity between the effects of water vapor and temperature can be avoided. They then linked the ray-tracing model and its tangent linear and adjoint operators into the Spectral Statistical Interpolation (SSI) analysis system of the National Centers for Environmental Prediction (NCEP). The new bending angle assimilation system was tested using over thirty actual GPS/MET observations (Zou et al. 2000). Liu et al. (2001) assessed the impact of assimilating the GPS bending angle on

Table 1. GPS level-2 information used for bending angle assimilation.

Data	Description
start_time	Starting time for the occultation
stop_time	Ending time for the occultation
year	The year during which this occultation ended
day	The day of year during which this occultation ended
MSL_alt	Mean Sea Level altitude
impact_parm	Impact parameter
bend_ang	Bending angle at perigee
lat	Longitude of perigee point
lon	Longitude of perigee point
az	Angle from the occultation plan in the direction of the GPS satellite with North

analyses and forecasts by incorporating 837 GPS/MET occultations for the period June 20–30, 1995. The impact on the global analysis was examined by comparing the analysis produced with the bending angles with 56 collocated radiosonde profiles. Analyses of the temperature and specific humidity above 850 hPa were closer to radiosonde measurements than the original guess fields. They also found that including the bending angles resulted in a small improvement in the short-range (6-h) and medium-range (one to five days) temperature forecast, especially in the Southern Hemisphere.

After this preliminary work on GPS data assimilation, further efforts were made to improve the accuracy and efficiency of GPS bending angle assimilation. Zou et al. (2002) carried out a statistical estimate of the errors in the calculation of bending angles caused by a 2D approximation of ray tracing and the assumption of spherical symmetry of the atmosphere. Shao and Zou (2003) studied the sensitivity of assimilating GPS/MET bending angles to the specification of observational weightings. They found that the temperature and the surface pressure are more sensitive than moisture to the specification of weightings. Liu and Zou (2003) improved the accuracy and efficiency of a 2D forward GPS ray-tracing model. The present work is based on the improved bending angle assimilation system.

3.2 *Experimental design*

We use the SSI analysis system of the NCEP for this study. Zou et al. (2000) describe the mathematical formulation of the 3D-Var problem. An incremental approach is used in which the inner loop solves a linear equation for the increment added at each outer loop using a standard linear conjugate-gradient algorithm (Parrish and Derber 1992). Data assimilation experiments are carried out at a horizontal resolution of T170 (approximately 100 km at the equator). In the vertical, there are a total of 42 σ-layers, with the model top located at about 2 hPa (40 km). Data assimilation is conducted at 6-h intervals. At each analysis time, two outer loops and 200 inner loops (100 for each outer loop) are carried out.

As was explained in Zou et al. (1999), GPS bending angles, as a function of the impact parameter $\alpha(a)$, are incorporated directly into the NCEP SSI system. Starting from the same background field at 00 UTC July 16, 2002, two data assimilation cycles are conducted. The first data assimilation cycle, NO-GPS, includes virtually all observations that were assimilated operationally at NCEP during that time period, except for the NOAA-16 AMSU radiance data[1]. The observations used are summarized at Table 2. The 6-h forecast initialized by the previous analysis is used as a guess field for the next analysis. The second data assimilation experiment, GPS, is the same as NO-GPS except

Table 2. The observations included in the NO-GPS experiment (after passing the SSI internal quality control and thinning procedures) on 00 UTC, July 16, 2002.

Data Type	Total number of observations
NOAA-15 HIRS 1b radiance	33978
NOAA-14 HIRS 1b radiance	27391
NOAA-15 AMSU-A 1b radiance	58629
NOAA-15 AMSU-B 1b radiance	103766
NOAA-14 MSU 1b radiance	5442
NOAA-16 SBUV ozone profile	187
GOES-8 5 $\times$ 5 cloud cleared radiance	6559
GOES-8 5 $\times$ 5 cloud cleared radiance	4724
q	10701
p_s	13451
T	53966
u, v	137625

1 These data were inadvertently omitted in our experiments. Omission of these data results in lower forecast skill scores than the NCEP operational forecasts and probably results in an overestimation of the impact of the CHAMP RO observations compared to the impact if the AMSU data were included in the experiments.

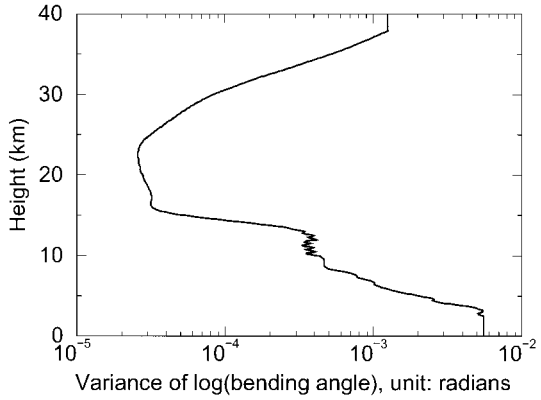

Fig. 2. Vertical variation of the estimated variance of the logarithm of bending angles.

that CHAMP bending angle observations are added.

A total of 229 out of 3030 CHAMP profiles occurred within a 3-h time window and a 200-km distance of conventional soundings (radiosonde and dropsonde profiles). These collocated conventional soundings, which are excluded from the assimilation in both experiments, are intended for an independent verification. Since the vertical resolution of the data assimilation system is much lower than that of the CHAMP measurements, the CHAMP bending angles are assimilated at selected levels, with an interval of 0.2 km below 3.2 km, 0.4 km between 3.2 and 10 km, 1 km between 10 and 20 km, and 2 km above 20 km. The average number of rays simulated for each occultation is 69.

The natural logarithm of bending angle ($\ln \alpha$) is used as the GPS observational quantity in the cost function J as in Zou et al. (2000). The weighting coefficients for the GPS data assimilation procedure are calculated as the inverse of the mean square difference between the observed and the simulated $\ln \alpha$, calculated from the background field-using a total of 4306 CHAMP occultations in May 2002. The mean square differences in terms of $\ln \alpha$ are shown in Fig. 2. The error variances compare favorably with the total bending angle errors estimated by Palmer et al. (2000). As tested in Shao and Zou (2003), such an estimate of the observation error variance based on observational increments produces a reasonably good result.

The observation operator for the bending angle assimilation consists of a ray-tracing model, whose basic physical concepts and numerical procedures were described in Zou et al. (1999). Several improvements made to the ray-tracing model were presented in Liu and Zou (2003). In the ray-tracing model, the Earth is assumed spherical with a single radius (r_{loc}) of local curvature for each occultation. At the tangent point, r_{loc} is related to the impact parameter through the following relationship:

$$a_t = n(z_{\mathbf{MSL}} + r_{\mathbf{loc}}) \tag{1}$$

where n is the index of refraction and z_{MSL} is the tangent point mean sea level height. At and above a height of 40-km height, $n \approx 1$. Therefore, the radius of the local curvature of the Earth for each occultation is calculated in the forward ray-tracing model as the difference between the impact parameter and the altitude of the ray:

$$r_{loc} = a_t|_{\mathbf{40\,km}} - Z_{\mathbf{MSL}} \tag{2}$$

where a_t and z_{MSL} are provided in the CHAMP level-2 data. This ensures the consistency in the calculation of the local curvature radius of the Earth between the ray-tracing model and the CHAMP data and therefore eliminates the need for an impact parameter offset that was present in our previous studies (Liu et al. 2001; Liu and Zou 2003). The ray integration starts from the observed perigee point and is carried out in two opposite directions, one toward the LEO satellite and the other toward the GPS satellite. This proves to be a more accurate scheme than the original scheme in which the simulated ray path starts from a virtual GPS position (Liu and Zou 2003). The newer technique ensures that the impact parameter and the tangent direction of a simulated ray at the perigee point, where the most bending of the ray occurs, are closer to the actual measurements than in the original technique.

4. Numerical results

We have combined the background state vectors and all other observations with and without bending angle profiles from CHAMP occultation observations from July 16$^{\text{th}}$ to July 31$^{\text{st}}$, 2002. The background state vectors are generated by 6-h forecasts using the NCEP global spectral model at T170L42 resolution. We first

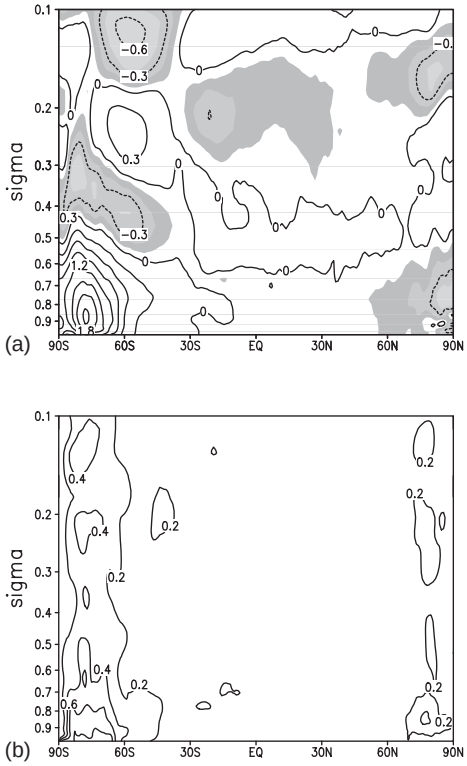

Fig. 3. (a) Zonal mean temperature differences between GPS and NO-GPS analyses averaged over the two-week period. (b) Zonal mean standard deviations of temperature difference between GPS and NO-GPS analyses. The contour interval is 0.3 K in (a) and 0.2 K in (b). Areas with values ≤ -0.1 K in (a) are shaded.

discuss the results in terms of temperature, specific humidity and surface pressure differences between the 3D-Var solutions with and without CHAMP GPS occultations. The 3D-Var results are then compared with collocated radiosonde and dropsonde observations in terms of temperature, specific humidity and surface pressure. The differences are expressed by the mean and the standard deviation on latitude versus height and/or longitude versus height cross sections.

4.1 Analysis differences

Figure 3 shows the zonal mean temperature differences between GPS and NO-GPS analyses averaged over the two-week period. The smaller temperature differences between the solution with and without CHAMP occultations in the Northern Hemisphere in Fig. 3 reflects the relatively smaller temperature errors in the Northern Hemisphere analysis compared to the Southern Hemisphere analysis in the absence of CHAMP occultations. The GPS analyses are significantly warmer than the NO-GPS analyses south of 30°S in the entire troposphere (except in a cold pocket between 45–85°S and approximately 300–500 hPa). Large temperature increases in the GPS solution are found in the middle and high latitudes. The maximum is over 2.1 K located around 80°S near the surface. It should be noted that the variation of surface height is very large around this latitudinal circle. There is a small low-latitude cooling impact between $\sigma = 0.3$ and $\sigma = 0.15$ in the GPS, indicating a better representation of the extremely cold temperatures at the tropopause by the high vertical resolution of GPS observations compared to the other satellite observations that are used in the analyses. Above the tropopause in the tropics, a weak systematic warming is also observed. Except for the lower troposphere near the north pole, the mean temperature changes introduced by CHAMP occultations are less than 0.3 K in the Northern Hemisphere. The standard deviations of the temperature changes in the Southern Hemisphere are also larger than in the Northern Hemisphere. The region of large standard deviations coincides with a region of large warming produced by the GPS observations in the Southern Hemisphere, indicating significant disagreement between the model and GPS observations in individual profile structures as well as their average. These results indicate a likely significant operational impact of RO observations in the Southern Hemisphere.

The average zonal mean specific humidity differences between GPS and NO-GPS analyses are shown in Fig. 4. The GPS solution is drier than the NO-GPS solution throughout the troposphere below 700 hPa and north of 30°S where the water vapor content is substantial in this season. The locations of the greatest water vapor changes are different from those of the temperature changes (compare Figs. 3 and 4). The maximum drying impacts of more than 0.2 g kg^{-1} occur near the north pole, 850 hPa, and in the northern subtropics around 900 hPa. The drying impact generally increases toward

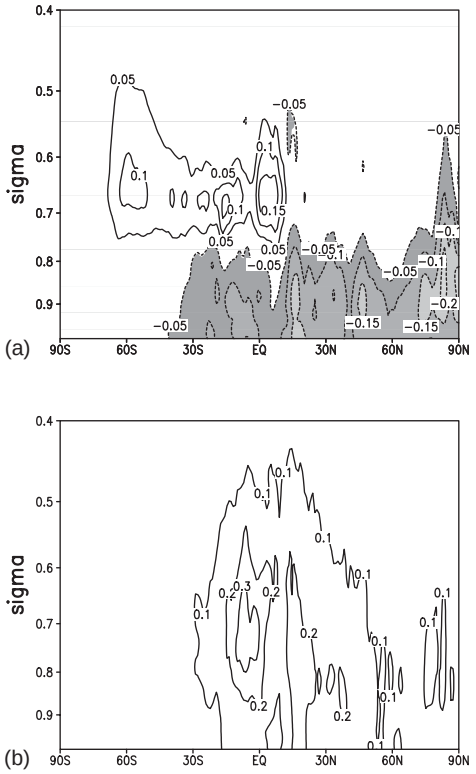

Fig. 4. Same as Fig. 3 except for specific humidity. The contour interval is 0.05 g kg^{-1} in (a) and 0.1 g kg^{-1} in (b). Areas with values ≤ -0.05 g kg^{-1} in (a) are shaded.

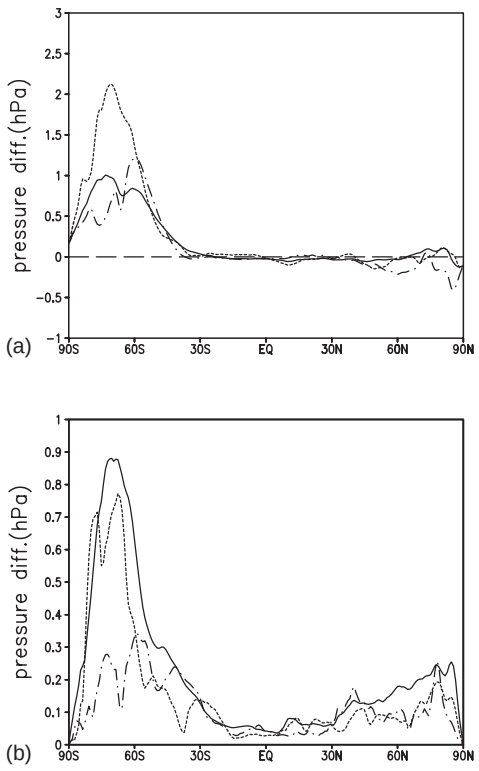

Fig. 5. (a) Latitude dependence of the mean surface pressure differences between GPS and NO-GPS analyses averaged over the two-week period. (b) Latitude dependence of zonal mean standard deviations of surface pressure difference between GPS and NO-GPS analyses. The solid line is for average over all longitudes, the dashed line is for the average from 180°E to 120°W, and the dot-dashed line is from 70° to 130°E. Also indicated in (a) is the long-dashed zero line.

low latitudes. These results are consistent with those of Kursinski and Hajj (2001), who found that the GPS/MET RO observations below 6 km are generally drier than the ECMWF analyses, with the difference generally increasing toward warmer temperatures. Above about 700 hPa, the GPS analysis is wetter than the NO-GPS analysis, with the largest increase of specific humidity (> 0.1 g kg^{-1}) primarily located in the Southern Hemisphere between 0°–60°S and just north of the equator near 650 hPa.

Kursinski and Hajj (2001) found that the GPS/MET observations are more moist than the NCEP analyses in the lower troposphere of low latitudes (10 S–30 N), which is not seen in our GPS analyses (Fig. 4). Since the moistening impact of the GPS/MET observations in this region was not found with the ECMWF analyses by Kursinski and Hajj (2001), we believe this difference in the GPS impact on the NCEP analyses between our study and that of Kursinski and Hajj (2001) in this region results from the reduced dry bias in the NCEP analyses since 1995, as well as the limited number of GPS/MET profiles probing the low-latitude, near-surface environment. In addition, different approaches used in both studies may also contribute to this disagreement. Standard deviations are largest at the equator, reaching a peak value of more than 0.3 g kg^{-1}, near 5°S and 700 hPa.

Figure 5 shows the latitudinal dependence of the zonal mean differences between GPS

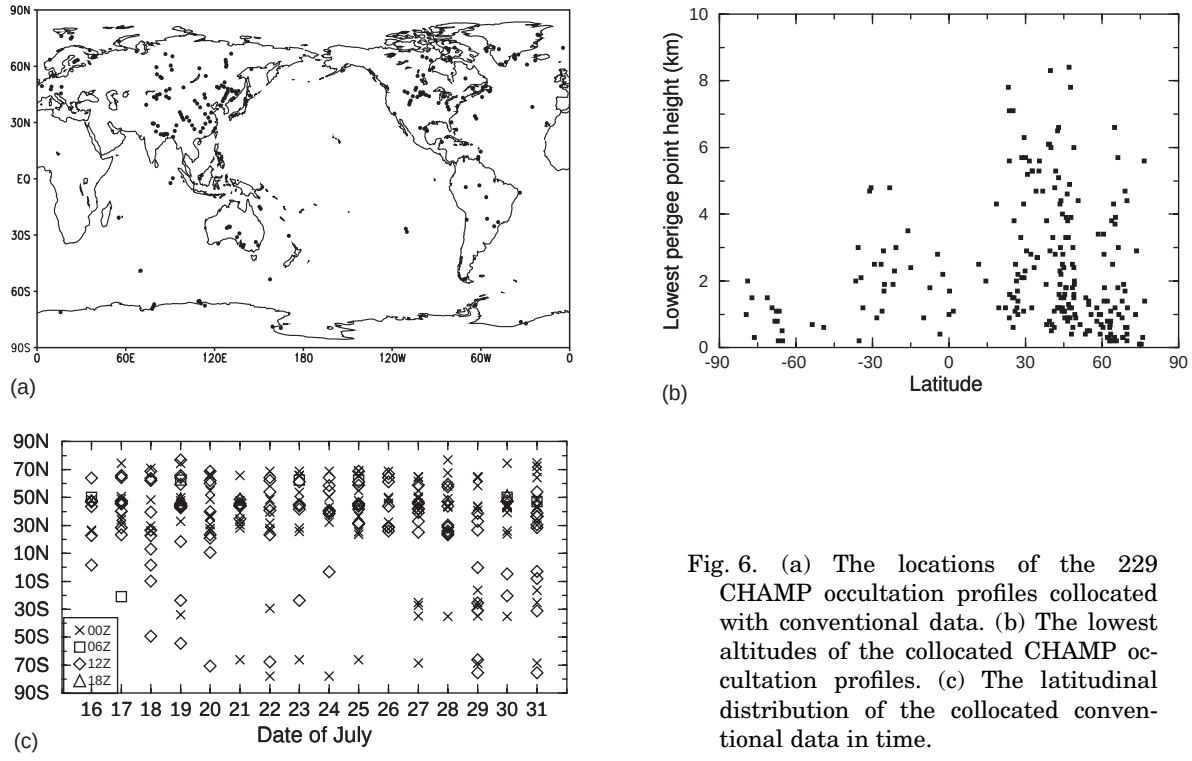

Fig. 6. (a) The locations of the 229 CHAMP occultation profiles collocated with conventional data. (b) The lowest altitudes of the collocated CHAMP occultation profiles. (c) The latitudinal distribution of the collocated conventional data in time.

and NO-GPS surface pressure analyses. In the Northern Hemisphere, where there are relatively many radiosonde and surface observations, the GPS analysis is close to the NO-GPS analysis. In the Southern Hemisphere, the mean surface pressure from the GPS solution is larger than that of the NO-GPS solution. The larger magnitude of surface pressure impact in the Southern Hemisphere compared to the Northern Hemisphere is a result of a larger bias in the background bias in the Southern Hemisphere. The standard deviations of the surface pressure differences between the GPS and NO-GPS solutions (Fig. 5b) reach a maximum of approximately 1.0 hPa, which is consistent with the surface pressure analysis error estimate.

In order to examine the effect of the dense radiosonde network in the Northern Hemisphere, which imposes additional constraints on the surface pressure analysis, we calculated the surface pressure analysis differences between GPS and NO-GPS over a data-void area in the Pacific (180°W–120°E) and a data-dense longitudinal band (70°E–130°E) (Fig. 5). Results in Fig. 5 indicate that the mean surface pressure difference between GPS and NO-GPS is very small in both longitudinal bands in the Northern Hemisphere.

4.2 Analysis verification with collocated radiosonde and dropsonde observations

Out of 3030 CHAMP occultations, there are 229 occultations with at least one collocated radiosonde and/or dropsonde profile that has more than five levels of data and is observed within a $\pm$3-h time window and a 200-km distance. In order to conduct an independent verification for the bending angle assimilation, we excluded these collocated radiosonde and dropsonde observations (a total of 264) from both experiments (NO-GPS and GPS). The locations of these CHAMP occultations are shown in Fig. 6a; the lowest perigee point heights of these occultations are shown in Fig. 6b; and the latitudinal distributions of collocated radiosondes in time are shown in Fig. 6c. Most of the conventional observations selected for verification are located in the middle latitudes of the Northern Hemisphere. Many of the CHAMP

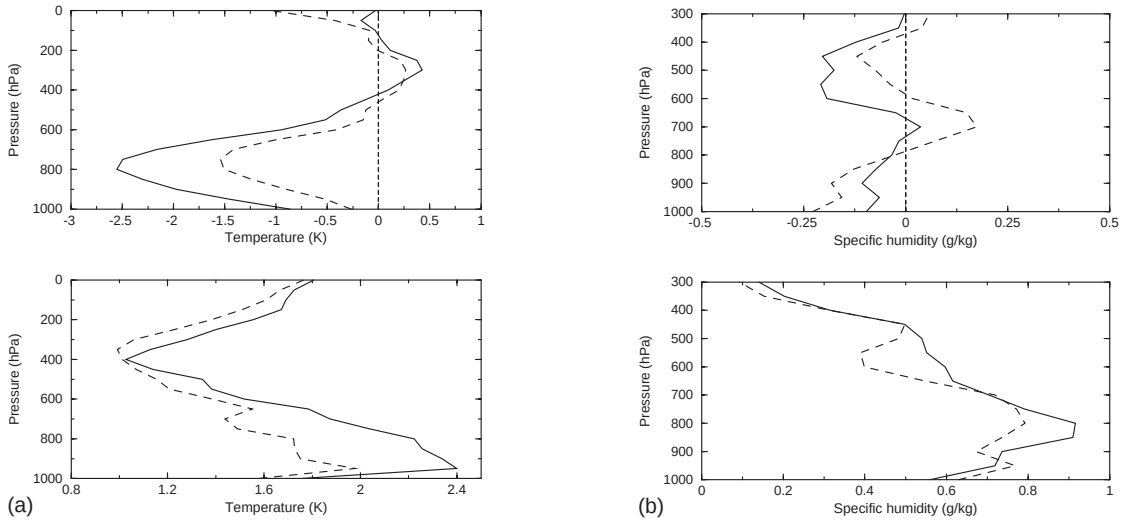

Fig. 7. (a) The mean (upper panel) and the standard deviation (bottom panel) of temperature differences between the analyses and the collocated radiosonde observations in the Southern Hemisphere. The solid line is for NO-GPS analyses and dashed line for GPS analyses. (b) Same as (a) except for specific humidity.

occultations reach to very low altitudes (at least 30 reached below 1.0 km). For comparisons between the analyses and conventional observations, the analyses are interpolated to the locations of observations.

The mean and standard deviations of the differences between the temperature and specific humidity analyses obtained by NO-GPS and GPS and the independent soundings are presented in Figs. 7–8. Comparisons are made for two areas: the relatively data-rich North America (15–90°N, 40–120°W) and the relatively data-poor Southern Hemisphere (10–90°S, 0–360°E). In the Southern Hemisphere, analyses without CHAMP data are systematically colder than conventional observations below 400 hPa (solid line in Fig. 7a). The cold bias in the GPS analyses is significantly reduced (a 40% reduction). In the upper troposphere, the analyses without GPS observations are slightly warmer than conventional observations. This warm bias is reduced slightly when GPS observations are assimilated. The GPS analyses near the top (0–50 hPa) of the atmosphere are colder than the NO-GPS analyses and conventional observations, which is probably a result of a GPS observational bias at these high altitudes. The differences between NO-GPS and GPS temperature analyses in North America (Fig. 8) are much smaller than in the Southern Hemisphere (Fig. 7). Both the biases and standard deviations of the differences are reduced by assimilating GPS observations.

The impact of CHAMP data on the water vapor analyses in the Southern Hemisphere and North America varies with altitude (Fig. 7b and 8b). The results are difficult to interpret because the radiosondes tend to have a dry bias in the upper troposphere. Furthermore, water vapor can vary greatly over spatial scales smaller than 200 km, and so radiosondes can have significant representativeness errors compared to large-scale analyses (Kuo et al. 2003). However, the mean differences in all cases are small (generally less than 0.25 g kg^{-1}). Adding CHAMP observations in both the Southern Hemisphere and North America increases the mean amount of water vapor in the analyses compared to the radiosondes above 800 hPa and dries the analyses below this level. The standard deviations of the differences in the analyses compared to radiosondes are reduced at all levels, except near the surface. The negative *N*-bias found in RO observations in the moist lower troposphere (Rocken et al. 1997; Kuo et al. 2003) may contribute to the observed drying of the analyses in the lower troposphere. Future GPS RO observations with the adoption

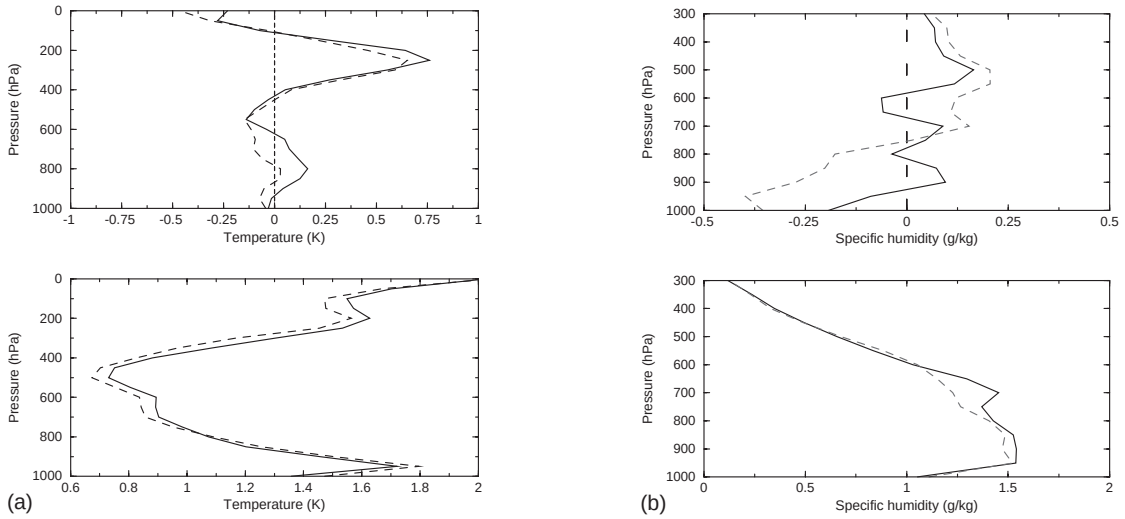

Fig. 8. (a) Same as Fig. 7a except for the North America area (15°–70°N, 40°–120°W). (b) Same as Fig. 7b except for the North America area.

of open-loop tracking and the removal of the navigation modulation from the GPS signal will significantly reduce such a bias (Ao et al. 2003).

4.3 Forecast results with and without CHAMP occultations

Five-day forecast experiments initialized with GPS and NO-GPS analyses at 12 UTC from July 16th to July 31st, 2002 are carried out using the NCEP global spectral model at T170L42 resolution (same resolution as the data assimilation experiments). Figure 9 shows the root-mean-square (RMS) error of geopotential height at 500 hPa, specific humidity at 850 hPa and surface pressure in the Southern Hemisphere. Figures 10–11 show the anomaly correlation of geopotential height at 500 hPa in the Southern Hemisphere. Figure 12 presents the RMS error of geopotential height at 500 hPa and specific humidity at 850 hPa in the Northern Hemisphere tropics (0–30°N). Results in the Southern Hemisphere are calculated over traditional verification areas (i.e., 20–80°S) following the NCEP's standard procedure. The GPS analyses are used as verification dataset for the RMS calculations and the NCEP climatology is used for anomaly calculation. Marginal, but discernable improvements in the forecast skill are seen in both hemispheres. A further breakdown in terms of spatial scales in AC scores reveals that the

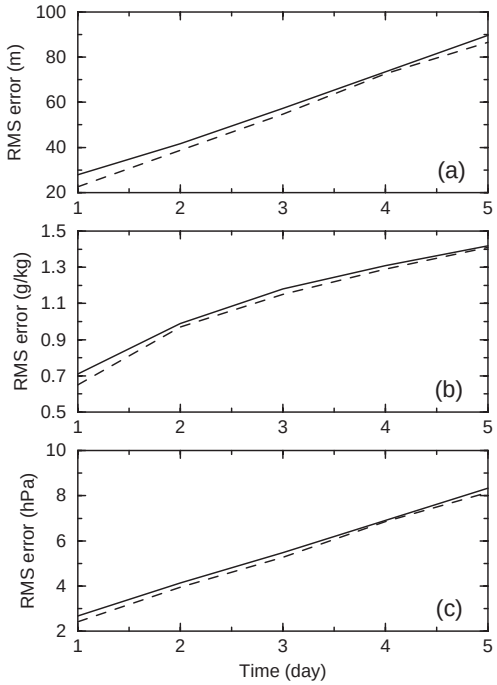

Fig. 9. The RMS errors of (a) 500 hPa geopotential height, (b) 850 hPa specific humidity, and (c) surface pressure forecasts in the Southern Hemisphere from one to five days. The solid line is for the NO-GPS forecasts, and the dashed line is for the GPS forecasts.

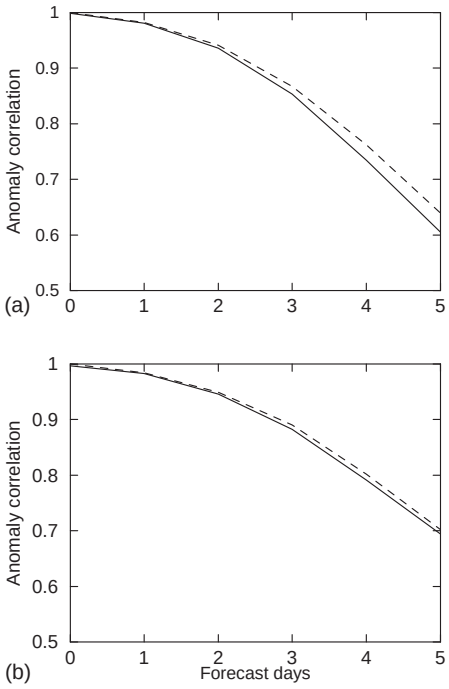

Fig. 10. The anomaly correlations of 500 hPa geopotential height forecasts in the Southern Hemisphere from one to five days: (a) Wave number 4–9, and (b) all waves (waves 1–20). The solid line is for the NO-GPS forecasts, and the dashed line is for the GPS forecasts.

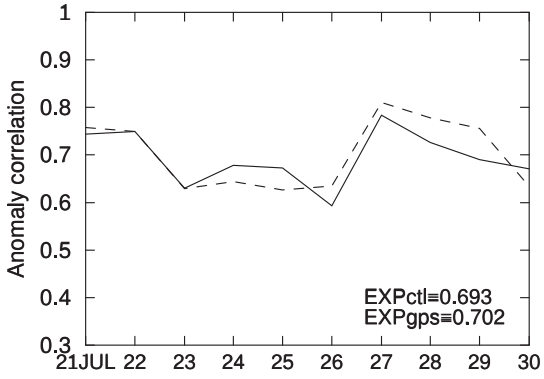

Fig. 11. Daily variation of the anomaly correlations of 500 hPa geopotential height forecasts in the Southern Hemisphere at day five (all waves from 1 to 20). The solid line is for the NO-GPS forecasts, and the dashed line is for the GPS forecasts.

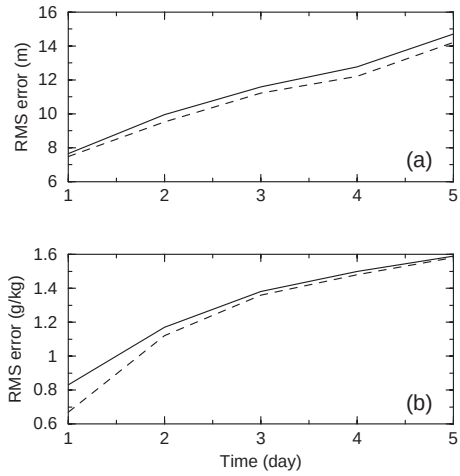

Fig. 12. Same as Fig. 9a–b except for the Northern Hemisphere tropics (0°–30°N).

improvements mainly come from a better description of the evolution of synoptic scales. In the daily performance scores shown in Fig. 11, the advantage of including the GPS observations stands out much more clearly after about one week, which we consider to be the forecast analysis spin-up time period. No substantial impact is found in the Northern Hemisphere north of 30°N (not illustrated).

In order to examine the impact of 6-h continuous cycling, we have plotted the daily variation of the RMS error of the 500-hPa height for five forecast days from July 16th to July 31st, 2002 in the Southern Hemisphere (Fig. 13). A more significant impact of CHAMP RO observations is observed during the second week of the continuous data assimilation cycling than within the first week of the cycle, especially for the day-1 and day-2 forecasts. In other words, with the current CHAMP data density, it seems to take about one week for the analysis to be "spun-up" and to show an impact on the Southern Hemisphere.

The GPS analyses are used for verification of forecasts shown in Figs. 9–13. Figure 14 shows the rms error of the five-day forecasts initialized with both the NO-GPS and GPS analyses verified with the NCEP operational analyses. The rms error of the NCEP operational forecasts is also shown in this figure (dash-

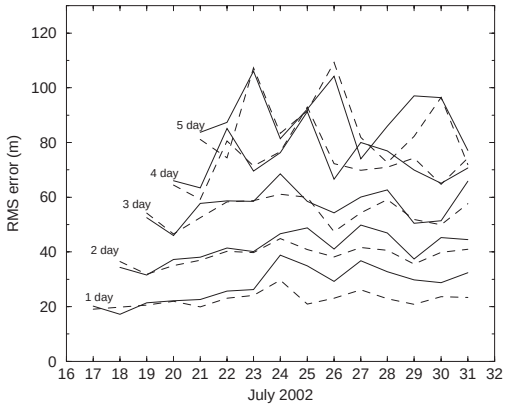

Fig. 13. Daily variation of the RMS error of the 500-hPa height for forecast days one, two, three, four and five from July 16th to July 31st, 2002 in the Southern Hemisphere. The solid line is for the NO-GPS forecasts, and the dashed line is for the GPS forecasts.

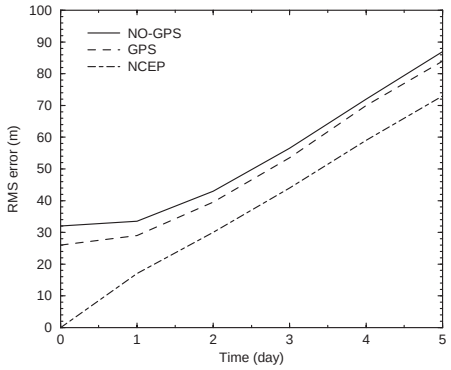

Fig. 14. The RMS errors of 500 hPa geopotential height forecasts in the Southern Hemisphere from one to five days verified against the NCEP operational analyses. The solid line is for the NO-GPS forecasts, the dashed line is for the GPS forecasts, and the dash-dotted line is for the NCEP operational forecasts.

dotted line). As seen clearly, forecasts initialized with either NO-GPS or GPS analyses are not as skillful as the NCEP operational forecast due to the omission of AMSU radiance data in these two experiments. However, the addition of CHAMP GPS RO observations reduces the rms forecast error in the Southern Hemisphere even when the NCEP operational analyses are used for verification.

5. Summary and conclusions

The German/US CHAMP mission, carrying a new generation GPS receiver, has provided about 200 RO observations daily since February 11, 2001. Almost fifty percent of CHAMP occultations descend to a height lower than 850 hPa, which alleviates one of the limitations of the GPS/MET experiments. The CHAMP observations allow the added value of RO observations to global analyses and forecasts to be assessed using a recently improved observation operator and the 3D-Var system for assimilating GPS RO bending angles.

The impact of RO observations on global analyses and forecasts are assessed in the presence of other observations (excluding the NOAA-16 AMSU radiances) for the first time. The NCEP SSI analysis system is used for data assimilation, and the NCEP global spectral model is used for forecasts. Both data assimilation and forecast experiments are conducted at T170L42 resolution. CHAMP RO bending angles from July 16th to July 31st, 2002 are included in the NCEP SSI analysis system. A total of 3030 occultations that were processed by UCAR CDAAC during this period are included in a two-week data assimilation cycle. Of the 3030 total CHAMP profiles, 229 occurred within a $\pm$3-h time window and a 200-km distance of at least one radiosonde or dropsonde profile. These collocated in-situ observations are excluded from both data assimilation experiments for evaluation purposes. Analyses produced with CHAMP bending angle observations are compared with analyses produced without CHAMP observations. The following are major findings:

1. The analyzed temperatures in the Southern Hemisphere become higher when CHAMP data are included. Since the analyses without CHAMP observations have a cold bias error in the Southern Hemisphere, inclusion of CHAMP observations reduces this cold bias significantly.
2. When CHAMP observations are included, the analyzed water vapor decreases in the lower troposphere (below 700 hPa) and increases in the middle troposphere (400–

700 hPa), particularly in the mid-latitudes of the Southern Hemisphere, the tropics and the subtropics. Adding CHAMP observations in both the Southern Hemisphere and North America increases the mean amount of water vapor in the analyses compared to independent soundings above 800 hPa and dries the analyses compared to the soundings below this level.

3. Inclusion of CHAMP observations does not produce significant changes in the average surface pressure analysis in the Northern Hemisphere. However, a slight increase of the average surface pressure (maximum 1 hPa) is observed in the Southern Hemisphere.
4. One- to five-day forecasts initialized with and without CHAMP observations demonstrate that the forecast skill is improved slightly with the inclusion of CHAMP data in the Southern Hemisphere and in the Northern Hemisphere tropics.

It appears that the number of CHAMP observations is still too small (about 25 occultations within a 6-h time window in the Northern Hemisphere) to make a significant difference in the Northern Hemisphere analyses. Problems associated with humidity analysis in the lower troposphere for GPS data assimilation, which may be related to the negative N-bias in some of the CHAMP data, need to be studied further. The COSMIC constellation of six satellites, to be launched in late 2005, will provide up to 3000 soundings per day globally (Rocken et al. 2000). The COSMIC mission will enable the testing of the impact of a large number of RO soundings on operational NWP in real time.

Acknowledgments

This research is supported by the National Science Foundation under the project ATM-0101036 and the Integrated Program Office of NOAA's National Polar-orbiting Operational Environmental Satellite System under SMC/CIPN Project Order No. Q000C1737600086. The authors would like to thank Dr. Doug Hunt for providing CHAMP data and technical consultation and Dr. Sergey Sokolovskiy for providing us the code of vector rotation. The authors would also like to thank Dr. Steve Lord at NCEP for his support to use the NCEP SSI system in this work. Finally, we thank Dr. Y.-H. Kuo for his review of the manuscript and helpful comments.

Appendix A

Computation of the normal vector of the occultation plane using CHAMP level-2 data

The normal vector of an occultation plane is a required input quantity of the ray-tracing operator. It was directly provided in the GPS/MET data sets. Instead of the normal vector, the azimuth angle at the perigee point of an occultation is provided by the CHAMP data sets. In the following, we first explain the azimuth angle provided by CHAMP and then derive the normal vector of an occultation plane from its azimuth angle and perigee point position, which are both provided in the CHAMP level-2 data set (see Table 1).

The azimuth angle in CHAMP data is described as "the angle from the occultation plane in the direction of the GPS satellite with the north direction". Figure 15 illustrates schematically several important geometrical features associated with a ray path, which goes from a GPS satellite to a LEO satellite, including the azimuth angle. Point P_t is the perigee point. The center of the local curvature is denoted as O. The vector from O to P_t is called the perigee point position vector (denoted by $\mathbf{r}_t$). A sphere with its origin at O and radius $|\boldsymbol{r}|$ can be drawn. The perigee point P_t is on the surface of this sphere. Two planes are considered. The first one is the occultation plane, which is defined by the center of the local curvature and the LEO and the GPS satellite positions. The second one is a meridian plane, which is defined by the center of the local curvature, the perigee point and the north pole. The occultation plane, the meridian plane and the spherical surface intersect at P_t. We introduce two unit vectors starting at P_t: $\mathbf{u}^t_{occ}$ and $\mathbf{u}^t_{mer}$. The vector $\mathbf{u}^t_{occ}$ is a unit vector opposite to the tangent direction of the ray at the perigee point, i.e., it points from the perigee point in the direction of the GPS satellite and is tangent to the sphere at the tangent point. The vector $\mathbf{u}^t_{mer}$ points from the perigee point in the direction of the north pole, and is also tangent to the sphere at the perigee point. The vector $\mathbf{u}^t_{occ}$ lies in the occultation plane and

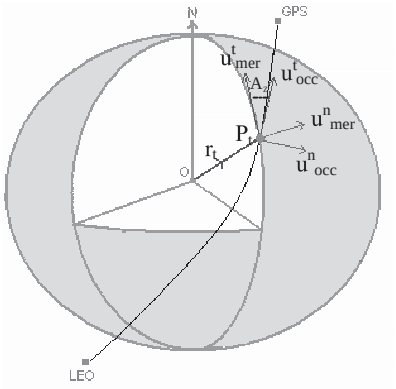

Fig. 15. Schematic illustration of the azimuth angle and other vectors used in the computation of the unit vector normal to the occultation plane. A ray passes through the atmosphere from a GPS satellite to a LEO satellite. P_t is the perigee point of the ray. O is the center of the local curvature. With O as the origin, a sphere is defined as passing through the tangent point P_t. Two major planes, the meridian plane and the occultation plane, intersect the sphere at the perigee point. The tangent vectors at P_t in these two planes are defined as $\mathbf{u}^t_{mer}$ and $\mathbf{u}^t_{occ}$. $\mathbf{u}^t_{mer}$ is the unit tangent vector in the meridian plane, pointing from P_t in the direction of the local north. $\mathbf{u}^t_{occ}$ is the unit tangent vector in the occultation plane, pointing from P_t in the direction of the GPS satellite. $\mathbf{u}^n_{mer}$ and $\mathbf{u}^n_{occ}$ are the unit vectors normal to the meridian plane and the occultation plane, respectively. The angle between $\mathbf{u}^t_{mer}$ and $\mathbf{u}^t_{occ}$ is the azimuth angle (A_z) of the occultation plane defined in the CHAMP data. It can be shown that the angle between $\mathbf{u}^n_{mer}$ and $\mathbf{u}^n_{occ}$ is equivalent to the angle between $\mathbf{u}^t_{mer}$ and $\mathbf{u}^t_{occ}$.

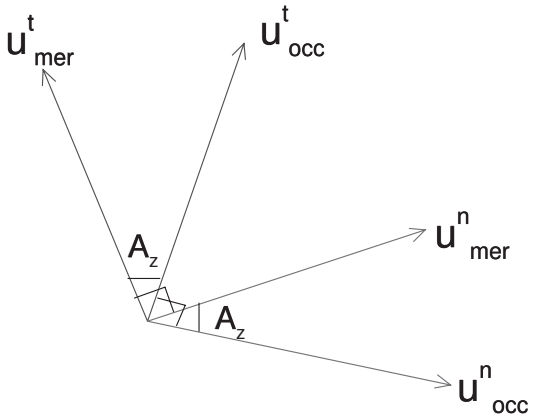

Fig. 16. A local Cartesian coordinate. The coordinate center is at P_t. The vertical axis z' is in the direction of $\mathbf{r}_t$ and the $x'-y'$ plane is defined by $\mathbf{u}^n_{mer}$ and $\mathbf{u}^n_{occ}$ with the x' axis in the direction of $\mathbf{u}^n_{occ}$. The angle between $\mathbf{u}^n_{mer}$ and $\mathbf{u}^n_{occ}$ (the x' axis) is equal to the azimuth angle (A_z) of the ray. Therefore, $\mathbf{u}^n_{occ}$ can be obtained by rotating $\mathbf{u}^n_{mer}$ around $\mathbf{r}_t$ by an angle A_z in a clockwise manner in the $x'-y'$ plane.

the vector $\mathbf{u}^t_{mer}$ lies in the meridian plane. We notice that the direction of $\mathbf{u}^t_{mer}$ is the local direction of north at the perigee point. Thus, according to its definition, the azimuth angle A_z provided by CHAMP data is the angle between $\mathbf{u}^t_{occ}$ and $\mathbf{u}^t_{mer}$ (see Fig. 15). If the vector normal to the occultation plane $(\mathbf{u}^n_{occ})$ and the vector normal to the meridian plane $(\mathbf{u}^n_{mer})$ are defined at the right hand side of the vectors $\mathbf{u}^t_{occ}$ and $\mathbf{u}^t_{mer}$, respectively, the angle between these two normal vectors is equal to A_z based on simple geometrical relationships shown in Fig. 16.

Having introduced the relationships among $\mathbf{u}^t_{occ}, \mathbf{u}^t_{mer}, \mathbf{u}^n_{occ}, \mathbf{u}^n_{mer}$, and A_z, it is easy to show how the normal vector $\mathbf{u}^n_{occ}$ can be calculated from the known azimuth angle and the position of the perigee point on the sphere. Since the perigee point position vector $\mathbf{r}_t$ lies in both the meridian plane and the occultation plane, it is perpendicular to both $\mathbf{u}^n_{occ}$ and $\mathbf{u}^n_{mer}$. A local Cartesian coordinate system (x', y', z') can be defined as shown in Fig. 17. The center of the coordinates is at the perigee point P_t. The vertical axis (z') is defined by $\mathbf{r}_t$, the x'-axis is defined by $\mathbf{u}^n_{occ}$, and the y'-axis is 90° anticlockwise of the x'-axis in the plane defined by $\mathbf{u}^n_{occ}$ and $\mathbf{u}^n_{mer}$. Since $\mathbf{u}^n_{occ}$ can be obtained by rotating $\mathbf{u}^n_{mer}$ around the z'-axis clockwise by an angle of $A_z, \mathbf{u}^n_{occ}$ can be expressed mathematically as

$$\mathbf{u}^n_{occ} = \mathbf{R} \cdot \mathbf{u}^n_{mer}, \tag{3}$$

where $\boldsymbol{R}$ is a 3-dimensional rotation matrix around the axis z' by an angle A_z in the clockwise direction.

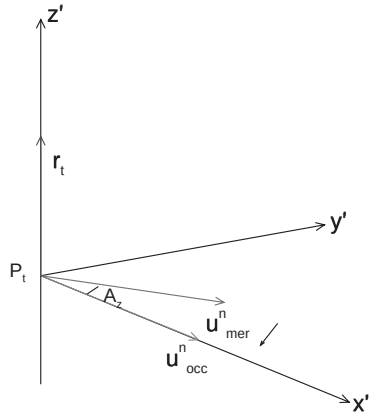

Fig. 17. Schematic illustration of a local Cartesian coordinate with its origin defined at the tangent point (P_t). The vertical z'-axis is in the direction of $\mathbf{r}_t$, the x'-axis is defined by $\mathbf{u}^n_{occ}$, and the y'-axis is in the plane defined by $\mathbf{u}^n_{occ}$ and $\mathbf{u}^n_{mer}$. Since the angle between $\mathbf{u}^n_{occ}$ and $\mathbf{u}^n_{mer}$ is equal to the azimuth angle (A_z), $\mathbf{u}^n_{occ}$ (the unknown vector) can be obtained by rotating $\mathbf{u}^n_{mer}$ (the known vector) clockwise by an angle A_z (known information) in the $x' - y'$ plane.

In a right-handed global Cartesian coordinate system defined at the origin O, the three components of the unit perigee point position vector $\mathbf{r}_t/|r_t|$ are functions of the geodetic latitude (ϕ) and longitude (λ) of the perigee point:

$$x_t = \cos\phi\cos\lambda, \tag{4}$$

$$y_t = \cos\phi\sin\lambda, \tag{5}$$

$$z_t = \sin\phi. \tag{6}$$

Similarly, the three components of the unit vector normal to the meridian plane, $\mathbf{u}^n_{mer}$ is

$$\mathbf{u}^n_{mer} = \begin{bmatrix} -\sin\lambda \\ \cos\lambda \\ 0 \end{bmatrix}. \tag{7}$$

The 3-dimensional rotation matrix $\boldsymbol{R}$ is (Glassner 1990)

$$\mathbf{R} = \begin{bmatrix} tx_t^2 + c & tx_ty_t - sz_t & tx_tz_t + sy_t \\ tx_ty_t + sz_t & ty_t^2 + c & ty_tz_t - sx_t \\ tx_tz_t - sy_t & ty_tz_t + sx_t & tz_t^2 + c \end{bmatrix}, \tag{8}$$

where

$$c = \cos A_z, \quad s = -\sin A_z, \quad t = 1 - \cos A_z. \tag{9}$$

Therefore, all values at the right hand side of the equation (3) can be derived from given CHAMP data using (4)–(9).

References

Ao, C.O., T.K. Meehan, G.A. Hajj, and A.J. Mannucci, 2003: Lower troposphere refractivity bias in GPS occultation retrievals. *J. Geophys. Res.*, **108**, 4577.

Engeln, A.v., G. Nedoluha, G. Kirchengast, and S. Buhler, 2003: One-dimensional variational (1-D Var) retrieval of temperature, water vapor, and a reference pressure from radio occultation measurements: A sensitivity analysis. *J. Geophys. Res.*, **108**, 4337–4349.

Eyre, J.R., 1994: Assimilation of radio occultation measurements into a numerical weather prediction system. *ECMWF*, *ECMWF Tech. Memo.*, **199**, 34pp.

Fjeldbo, G., G.A. Kliore, and V.R. Eshleman, 1971: The neutral atmosphere of Venus as studied with the Mariner V radio occultation experiments. *Astron. J.*, **76**, 123–140.

Glassner, A.S., 1990: *Graphics Gems*, Academic Press, 466pp.

Hajj, G.A., C.O. Ao, B.A. Iijima, D. Kuang, E.R. Kursinski, A.J. Mannucci, T.K. Meehan, L.J. Romans, M. de la Torre Juarez, and T.P. Yunck, 2003: CHAMP and SAC-C atmospheric results and intercomparisons. *J. Geophys. Res. Atmospheres*, (submitted).

Healy, S.B. and J.R. Eyre, 2000: Retrieving temperature, water vapor and surface pressure information from refractivity-index profiles derived by radio occultation: A simulation study. *Quart. J. Roy. Meteor. Soc.*, **126**, 1661–1683.

Kuo, Y.-H., S. Sokolovskiy, R. Anthes, and F. Vandenberghe, 2000: Assimilation of GPS radio occultation data for numerical weather prediction. *TAO*, **11**, 157–186.

———, T.-K. Wee, S. Sokolovskiy, C. Rocken, W. Schreiner, D. Hunt, and R.A. Anthes, 2004: Inversion and error estimation of GPS radio occultation data. *J. Meteor. Soc. Japan*, (submitted).

———, X. Zou, and W. Huang, 1997: The impact of GPS data on the prediction of an extratropical cyclone: An observing system simulation experiment. *J. Dyn. Atmos. Ocean.*, **27**, 439–470.

Kursinski, E.R. and G.A. Hajj, 2001: A comparison of water vapor derived from GPS occultations and global weather analyses. *J. Geophys. Res.*, **106**, 1113–1138.

Kursinski, E.R., S.B. Healy, and L.R. Romans, 2000: Initial results of combing GPS occultations

with ECMWF global analyses within a 1D-Var framework. *Earth, Planets and Space*, **52**, 885–892.

Liu, H. and X. Zou, 2003: Improvements to a forward GPS raytracing model and their impacts on assimilation of bending angle. *J. Geophys. Res.*, **108**, doi: 10.1029/2002 JD 003160, 2003.

———, ———, R.A. Anthes, J.C. Chang, J.-H. Tseng, and B. Wang, 2001: The impact of 837 GPS/MET bending angle profiles on assimilation and forecasts for the period June 20–30, 1995. *J. Geophys. Res.*, **106**, 31771–31786.

Melbourne, W.G., E.S. Davis, C.B. Duncan, G.A. Hardy, E.R. Kursinski, T.K. Meehan, L.E. Young, and T.P. Yunck, 1994: The application of spaceborne GPS to atmospheric limb sounding and global change monitoring. NASA and JPL, *JPL Publication 94-18*, 147pp.

Palmer, P.I., J.J. Barnett, J.R. Eyre, and S.B. Healy, 2000: A non-linear optimal estimation inverse method for radio occultation measurements of temperature, humidity and surface pressure. *J. Geophys. Res.*, **105**, 17513–17526.

——— and ———, 2001: Application of an optimal estimation inverse method to GPS/MET bending angle observations. *J. Geophys. Res.*, **106**, 17147–17160.

Parrish, D.F. and J. Derber, 1992: The National Meteorological Center's spectral and statistical-interpolation analysis system. *Mon. Wea. Rev.*, **120**, 1747–1763.

Poli, P., J. Joiner, and E.R. Kursinski, 2002: 1DVAR analysis of temperature and humidity using GPS radio occultation refractivity data. *J. Geophys. Res.*, **107**, 4448–4467.

Rocken, C., R. Anthes, M. Exner, D. Hunt, S. Sokolovskiy, R. Ware, M. Gorbunov, W. Schreiner, D. Feng, B. Herman, Y.-H. Kuo, and X. Zou, 1997: Analysis and validation of GPS/MET data in the neutral atmosphere. *J. Geophys. Res.*, **102**, 29849–29866.

———, Y.-H. Kuo, W.S. Schreiner, D. Hunt, S. Sokolovskiy, and C. McCormick, 2000: COSMIC system description. *TAO*, **11**, 21–52.

Shao H. and X. Zou, 2003: On the observational weighting and its impact on GPS/MET bending angle assimilation. *J. Geophys. Res.*, **107**, 1–28.

Tsuda, T., M. Mishida, C. Rocken, and R. Ware, 2000: A global morphology of gravity waves activity in the stratosphere revealed by the GPS occultation data (GPS/MET). *J. Geophys. Res.*, **105**, 7257–7273.

Ware, R., M. Exner, D. Feng, M. Gorbunov, K. Hardy, B. Herman, Y.-H. Kuo, T. Meehan, W. Melbourne, C. Rocken, W. Schreiner, S. Sokolovskiy, F. Solheim, X. Zou, R. Anthes, S. Businger, and K. Trenberth, 1996: GPS sounding of the atmosphere from low earth orbit: Preliminary results. *Bull. Am. Meteor. Soc.*, **77**, 19–40.

Wickert, J., C. Reigber, G. Beyerle, R. Konig, C. Marquardt, T. Schmidt, L. Grunwaldt, R. Galas, T.K. Meehan, W.G. Melbourne, and K. Hocke, 2001: Atmosphere sounding by GPS radio occultation: First results from CHAMP. *Geophys. Res. Lett.*, **28**, 3263–3266.

Yunck, T.P., C.H. Liu, and R. Ware, 2000: A history of GPS sounding. *Terrestrial, Atmospheric and Oceanic Science*, **11**, 1–20.

Zou, X., Y.-H. Kuo, and Y.-R. Guo, 1995: Assimilation of atmospheric radio refractivity using a non-hydrostatic adjoint model. *Mon. Wea. Rev.*, **123**, 2229–2249.

———, F. Vandenberghe, B. Wang, M.E. Gorbunov, Y.-H. Kuo, S. Sokolovskiy, J.C. Chang, J.G. Sela, and R. Anthes, 1999: A raytracing operator and its adjoint for the use of GPS/MET refraction angle measurements. *J. Geophys. Res.*, **104**, 22301–22318.

———, B. Wang, H. Liu, R.A. Anthes, T. Matsumura, and Y.-J. Zhu, 2000: Use of GPS/MET refraction angles in 3D variational analysis. *Quart. J. Roy. Meteor. Soc.*, **126**, 3013–3040.

———, H. Liu, and R.A. Anthes, 2002: A statistical estimate of errors in the calculation of radio occultation bending angles caused by a 2D approximation of raytracing and the assumption of spherical symmetry of the atmosphere. *J. Atmos. Ocean. Tech.*, **19**, 51–64.